Lab on a Chip

RSC Publishing

TECHNICAL INNOVATION

View Article Online
View Journal | View Issue

Size based sorting and patterning of microbeads by evaporation driven flow in a 3D micro-traps array†

Cite this: *Lab Chip*, 2013, **13**, 3663

Chee Chung Wong,*[a] Yuxin Liu,[ab] Karen Yanping Wang[a] and Abdur Rub Abdur Rahman[a]

Received 26th February 2013,
Accepted 2nd July 2013

DOI: 10.1039/c3lc50274k

www.rsc.org/loc

We present a three-dimensional (3D) micro-traps array for size selective sorting and patterning of microbeads *via* evaporation-driven capillary flow. The interconnected micro-traps array was manufactured by silicon micromachining. Microliters of aqueous solution containing particle mixtures of different sized (0.2 to 20 μm diameter) beads were dispensed onto the micro-traps substrate. The smaller particles spontaneously wicked towards the periphery of the chip, while the larger beads were orderly docked within the micro-traps array.

Microbeads technology has revolutionized biological assay in molecular and genomic research. The technology is advantageous as microbeads can be coated with an assay specific reagent, thereby facilitating high-throughput affinity based capture and detection of target biological molecules from a small sample volume.[1] Improved methods of tagging and handling microbeads have also allowed commercial products such as Luminex[2] and Ilumina[3] bead array technology to be used in applications of cancer diagnostics and drug discovery. Leveraging on the high-throughput of microbead array formats, microbead sorting and patterning technology would allow direct identification and mapping of analyte binding to size specific microbeads that are encoded with different target reagents. Microbeads with an added physical dimension such as bead sizes, can be utilized for detecting cytokines and simultaneously measuring multiple analytes for immunoassay or affinity assay. While several methods have been developed to trap microbeads in magnetic fields,[4] pillar structures,[5] and step structures,[6] these methods do not allow perfusion of additional reagents without disrupting the arrangement of particles from their original locations. In addition, a significant effort has been targeted at instrument-free microfluidic methods that eliminate the need for auxiliary instruments such as pumps, valves, and manifolds, in microfluidic assay implementation.[4–6] Several reports have been published on particle sorting through the use of capillary action[7] and surface tension driven pumping;[8] a force that can be generated with naturally occurring phenomena such as evaporation.[9,10]

The use of liquid evaporation to drive particles is attractive as it avoids dead volume loss associated with 2D membranes and weir or cross-flow filters[11] preclude the need to immunomagnetically tag particles for the sorting of mixtures.[12] In the context of systems that are based on micro-well arrays, there is frequently a need to introduce a new reagent after washing away the previous one for sequential reactions; an example of this occurs in microbead assays. Isolated micro-well arrays require pipetting of reagents in and out from the top, incurring dead volume at the bottom of the well. Furthermore, fluid introduction or removal within a closed system introduces chaotic hydrodynamic perturbations, increasing the possibility of disrupting particle arrangements.

The three-dimensional (3D) micro-traps array presented herein circumvents the above problems. We fabricated a 3D micro-traps filter array for sorting microliters of colloidal mixtures containing various particle sizes. A unique feature of this micro-traps array is size-selective docking and patterning of target particles induced by a radial inward flow during the movement of the receding meniscus.[13] With 3D micro-traps, an additional dimension of bead size would directly increase the number of analytes that are traditionally detected by colour coding. For example, size sorting and patterning of 3 different bead sizes in different trap regions, with red and green coded beads, would increase the number of analytes detected from 2 (red and green colour) to 6. The increase in analytes that could be simultaneously detected in a single assay would scale linearly as the equation $n \times x$, where n is the number of colour codes and x is the number of bead sizes. In addition, the approach has numerous advantages over dead end filtration techniques as it supports small volume liquid samples and offers size specific patterning of the microbeads. The micro-traps allow direct observation of the locality of the

[a]*Institute of Microelectronics, Agency for Science Technology and Research, 11 Science Park Road, Singapore Science Park 2, Singapore 117685, Singapore. E-mail: wongcc@ime.a-star.edu.sg; Fax: +65 6773 1914; Tel: +65 6770 5644*
[b]*School of Chemical and Biomedical Engineering, Nanyang Technological University, 62 Nanyang Drive, Singapore 637459, Singapore*

† Electronic supplementary information (ESI) available: Optical and fluorescence images of microbeads sorted and patterned on 3D micro-traps arrays. See DOI: 10.1039/c3lc50274k

microbeads and facilitate higher interaction between the target analyte and the microbeads, while offering open access. The surface-tension driven flow and concomitant receding meniscus in the 3D micro-traps allow size separation of microbeads. These phenomena were studied and verified by observing the evaporation of a 2 μl aqueous droplet containing a mixture of varying micron-sized particles. The sorting of particles in micro-fabricated silicon dioxide 3D micro-traps were observed with real-time optical microscopy and verified with scanning electron microscopy.

Working principle of surface tension driven flow

Fig. 1 schematically illustrates the principle of the evaporation driven self-sorting process for sorting particles of varying diameters in the 3D micro-traps array. When a microliter droplet of aqueous liquid containing a mixture of micron-sized particles is dispensed on the 3D array, the liquid wets the top surface forming a hemisphere (top droplet) and wets the gap between the traps (see illustrations in Fig. 1A and the cross sectional view in Fig. 1B). The surface tension driven flow operates based on the principle of a pressure difference between the droplet at the top of the chip and the sandwiched liquid film between the traps. This pressure difference is given by the Young–Laplace equation, $\Delta P = \gamma(1/R_1 + 1/R_2)$.[9] Where γ is the surface free energy of the liquid and R denotes the radius of curvature of the droplet at the liquid–air interface. Here R_1 is the radius of curvature of the droplet. In a non-spherical droplet such as the sandwich film, R_2 is approximated as half the width of the chip. This equation implies that the top droplet has a higher internal pressure as compared to the sandwiched liquid film beneath the traps. The consequence of this pressure difference is net liquid flow from the top droplet towards the periphery of the chip. As the top droplet evaporates and flattens over the array, a change in flow direction occurs when R_1 becomes larger than R_2.[14,15]

During beads sorting, the larger beads sediment quickly onto the top surface of the array, while the smaller beads remain in suspension inside the droplet. A liquid film fills the space between the top and bottom of the SiO_2 layer *via* capillary action. Surface tension driven flow transports finer beads outward from the centre of the top surface of the traps to the chip periphery. Evaporation occurs at the liquid/air boundary, shrinking the size of the liquid drop and thus causing the contact edge of the capillary film to recede. As the liquid drop evaporates, the randomly arranged larger beads are docked into the traps, as the meniscus of droplet recedes in a ring-like fashion. After the evaporation of the droplet, a ring of beads is formed on the top surface of the traps (see panel 4 in Fig. 1A): a phenomenon, known as the coffee-ring effect.[16] Once the entire sandwiched film has evaporated, the smaller beads can be seen aggregating around the periphery of the chip (see zoomed image of panel 4 in Fig. 1A).

Fabrication of the patterned 3D porous micro-traps

To fabricate the 3D micro-traps, we used a 200 mm silicon on insulator (SOI) wafer comprising of a 10 μm thick silicon layer

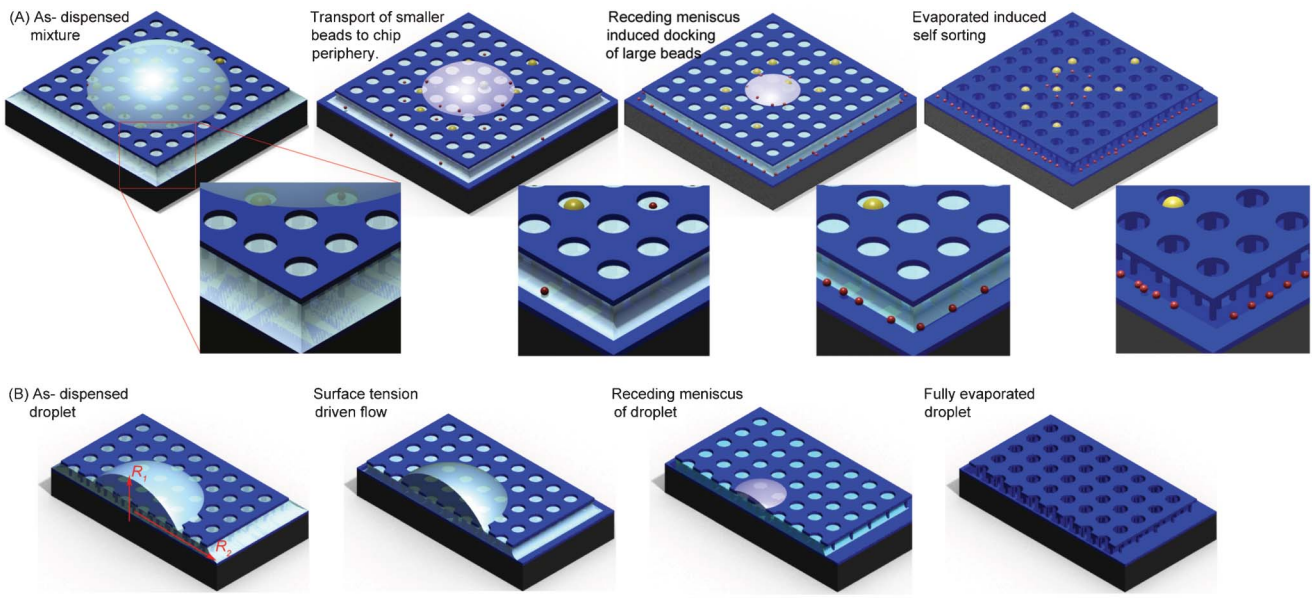

Fig. 1 Evaporation driven sorting and patterning of microbeads on 3D micro-traps. (A) As-dispensed droplet containing a mixture of yellow beads (16 μm) and red beads (2 μm). Surface tension driven flow from the droplet transports the smaller beads towards the periphery of the chip through the traps. Evaporation of the drop further triggers receding meniscus flow which pulls the larger beads into the micro-traps. Upon drying, arrays of large beads are patterned within the traps and the smaller beads are found aggregated at the bottom rim of the chip. Insets - zoomed images of 3D micro-traps. (B) Cross sectional view of the 3D micro-traps during evaporation of a pure water droplet as described in (A).

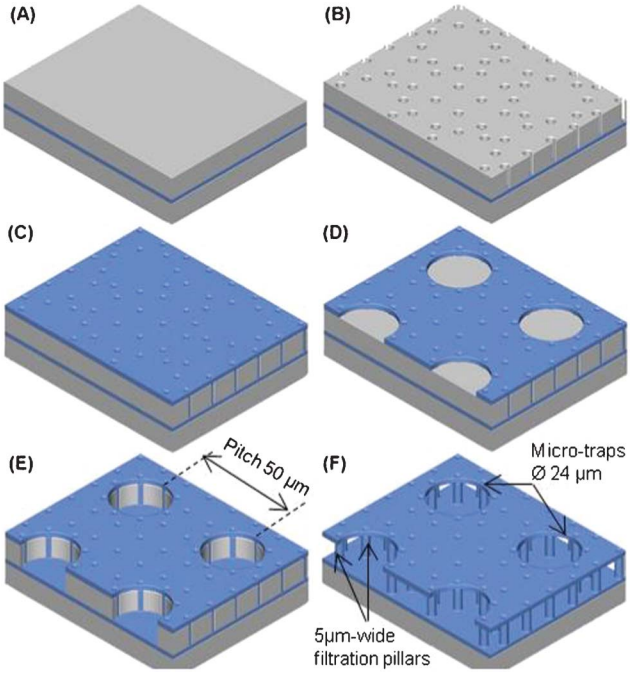

Fig. 2 Schematic of the fabrication process flow for the 3D micro-traps on silicon substrate. The blue and grey colour denotes the silicon dioxide (SiO_2) and silicon (Si) respectively.

and a sandwiched 1 μm-thick buried silicon dioxide (BOX) on silicon substrate (see Fig. 2A). The pillars having diameters of 4 μm and depths of 10 μm were defined by photolithography. Fig. 2B depicts the formation of circular vias on the silicon device layer etched using deep reactive ion etching (DRIE), which was stopped at the BOX layer. The photoresist was stripped with O_2 plasma and the polymeric residues from the wafers were cleaned in Piranha solution (H_2SO_4 : H_2O_2, 5 : 1) 125 °C. These via were filled with 2.5 μm thick of SiO_2 by plasma enhanced chemical vapor deposition PECVD at 400 °C (See Fig. 2C). The entrance of the micro-traps have an opening of 24 μm diameter to isolate beads 16 to 20 μm in diameter; these openings were patterned in the second photolithography step. The top layer PECVD SiO_2 was etched in a reactive ion etching tool using CHF_3 gas, as illustrated in Fig. 2D. The photoresist was stripped by O_2 plasma while the silicon layer was etched in DRIE (See Fig. 2E). The sacrificial silicon material was subsequently removed by isotropic etching with XeF_2 gas. Once released, the PECVD SiO_2 formed both the ceiling as well as the filtration pillars for the micro-traps (Fig. 2F). The exposed SiO_2 underneath the sacrificial silicon films formed the base of the traps for sorting of the finer microbeads.

The 3D micro-traps array consists of a 140 × 140 array with a footprint of 7 × 7 mm. The scanning electron micrograph (SEM) image of an array of released filters is shown in Fig. 3A. The traps on the top openings were spaced 50 μm apart while the filters beneath the traps had a gap size of 5 ± 0.2 μm. These 5 μm filters are used to trap medium size beads such as those between 6–10 μm in diameter, whilst filtering out the

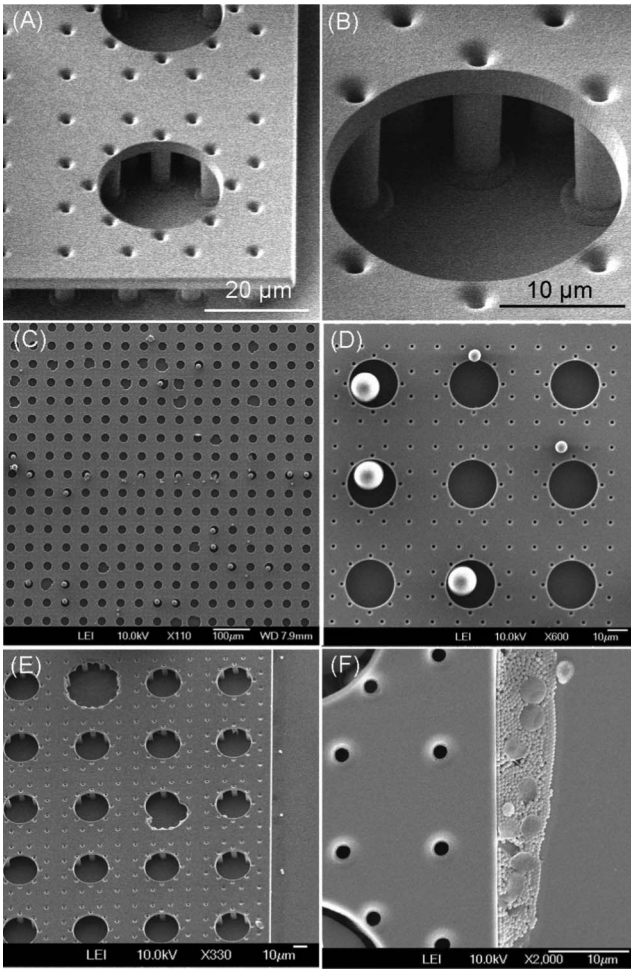

Fig. 3 Scanning electron micrograph of a fabricated 3D micro-traps filter. (A) 24 μm diameter trap with filter pillars. (B) Zoomed image of a single micro-trap. (C) Bead sorting and patterning of bead mixtures on a 140 × 140 micro-traps array. (D) Patterning of 16 μm beads after evaporation; some 6 μm beads are shown residing on the top surface. (E) 3 μm beads transported to the edge of the micro-traps after evaporation, and (F) zoomed image of sorted beads (0.2–1.0 μm) found beneath the edge of the array.

smaller ones. A zoomed image of a single trap is presented in Fig. 3B. The microfabrication techniques used allowed repeatable patterning of trap diameter of 24 μm with misalignment <0.5 μm. Microscopic analysis of fabricated micro-traps found that the morphological defect to individual traps occurred for one in thirty traps translating into a low error of <3% on the overall trapping efficiency. The 3D filter had a fill factor of 18%; calculated from the ratio of the total opening area accessible to traps to the entire area of array.

Results and discussion

The experiments comprised of: (i) sorting of smaller beads (1 μm, 2 μm, 3 μm, 4.5 μm, and 6 μm) from the 3D filters; (ii) docking and trapping of larger sized beads (6 μm, 8 μm, 10 μm, 16 μm, and 20 μm) in 3D micro-traps and lastly, (iii)

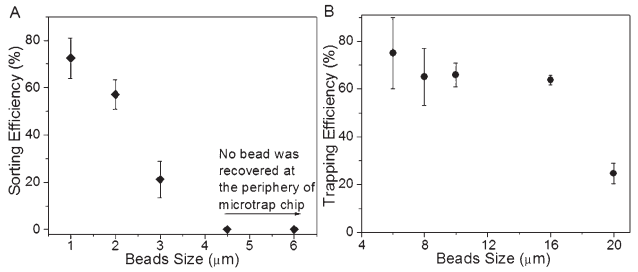

Fig. 4 Sorting and trapping efficiency of beads as a function of the bead's size. (A) Sorting efficiency of 1–6 μm diameter beads and (B) trapping efficiency of 6–20 μm diameter beads. Mean value ± SD (where n = 3).

patterning and sorting of model mixture of 2 μm, 6 μm, and 16 μm diameter beads. These polystyrene bead suspensions (PolyBead®, PolyScience Inc.) have concentrations ranging from 200 to 1000 beads/μl. Before the start of experiments, bead suspensions were subjected to five minutes of sonication to achieve uniform dispersion. A 2-μl droplet of the bead suspension was dispensed on top of the 3D micro-traps array using a pipette. Once the bead mixture was dispensed on top of the array, it wetted the top surface of the array and formed a drop with a contact angle of 15 ± 2 degrees. The wettability of the SiO_2 micro-traps array is comparable to the contact angles measured on planar SiO_2 glass surfaces (12 ± 3 degree).

Sorting efficiency is defined as the ratio of beads found at the periphery of the chips to the total number of beads seeded onto the array. The trapping efficiency is defined as the ratio of beads trapped within the array to the total number of beads seeded onto the array. The results for the sorting efficiency of 1 μm to 4.5 μm diameter beads are presented in Fig. 4A. Greater than 55% of 1 μm and 2 μm diameters beads were present at the periphery of the chip. Additional data on bead sorting are provided in Fig. S1(A–C), ESI.† The sorting efficiency decreases significantly for 3 μm diameter beads and it was observed that these beads interact more frequently with the pillars and sediment near stagnation points in the flow (see ESI,† Fig. S1D). Approximately 20% of the 3 μm diameter beads were sorted to the periphery while all the 4.5 μm diameters beads were all trapped within the 5 μm-spaced pillars. The latter has a trapping efficiency of 100% as no bead was found at the chip periphery. Fig. 3E shows three 3 μm diameter beads being transported by surface tension driven passive pumping to the periphery of the micro-traps array after evaporation.

In another experiment, a high concentration of 0.2–1.0 μm in diameter dyed beads were found sorted from the traps and located at the periphery of the chip (see Fig. 3F). The smaller beads sorted to the periphery of the chip could be dislodged by dipping the silicon chip in a bath of DI water. Alternatively, a filter paper could be placed around the periphery of the chip to wick out the eluent and facilitate the recovery of beads for further downstream analysis. In the trapping experiments, ~65% of 8 μm, 10 μm and 16 μm diameter beads were residing inside the 24 μm circular traps. Optical images of 3D micro-traps containing patterned microbeads from 6 μm to 20 μm diameter are presented in ESI,† Fig. S2. The larger 20 μm diameter beads have a lower trapping efficiency of 25%. In 8 μm diameter beads experiments, two beads were frequently observed in the same trap. The patterning efficiency for 6 μm diameter beads had a standard deviation >15% as the 24 μm diameter traps contained more than two beads residing inside each trap (see ESI,† Fig. S2A).

To demonstrate the capability of the micro-traps array to sort bead mixtures; a bead mixture containing beads of diameters 2, 6, and 16 μm was prepared and dispensed on the micro-traps array as previously described. A scanning electron micrograph of a fabricated 3D micro-traps filter revealed the docking of 16 μm beads inside the traps after evaporation, some 6 μm beads were also found on the surface (see Fig. 3D). The experimental results clearly demonstrated the effect of surface tension driven transportation of finer beads to the edge of the micro-traps array. This was evidenced in the form of a peripheral ring of microbeads driven by the drying of the liquid droplet, whilst the larger beads were trapped within the micro-traps array. Additional optical images of beads are provided in ESI,† Fig. S3. In a population set of n = 309, 205 beads of 16 μm diameter were patterned and trapped within the ordered array while 104 beads resided above the traps. The current receding meniscus approach achieved a patterning efficiency of >60% for 16 μm beads. Smaller 6 μm diameter beads were found trapped within the pillars and in some cases, two or more of these beads were found within single micro-traps (see Fig. 3C). Sorting of smaller beads was triggered by surface tension driven flow from the top droplet to the chip periphery while the docking of larger beads towards the circular traps was driven by receding meniscus flow.

Conclusions

This work highlights a pumpless microfluidic technique for the separation and sorting of particles within colloidal mixtures. The 3D micro-traps array enables patterning and geometric immobilization of larger beads, while allowing subsequent fluidic manipulation with multiple reagents without disturbing the geometric pattern. The 3D micro-traps array also filters out smaller diameter beads while retaining larger ones, which would be useful in applications like bead microarray assays. Greater than 60% trapping efficiency was recorded for polystyrene beads of 16 μm diameter, whereas a sorting rate of ~70% was recorded for the small 1 to 2 μm diameter beads. We believe that the simplicity and robustness of this approach makes it extremely appealing, especially for open access based sorting devices and bead manipulation in a high throughput manner (see detailed benchmarking of technology in ESI,† Table S1). The micro-traps array simultaneous traps and sorts beads based on size and has the potential to significantly increase throughput in bead assays.

Acknowledgements

This work was supported by the Agency for Science Technology and Research (Grant. 112 148 0002). The authors would like to show their appreciation for fabrication support from Vasarla Nagendra Sekhar and Marco A. D. Tocchetto, and editorial work done by Chaitanya Kantak.

References

1 K. Braeckmans, S. C. De Smedt, M. Leblans, R. Pauwels and J. Demeester, *Nat. Rev. Drug Discovery*, 2002, **1**, 447–456.
2 U. Prabhakar, E. Eirikis and H. M. Davis, *J. Immunol. Methods*, 2002, **260**, 207–218.
3 K. Kuhn, S. C. Baker, E. Chudin, M. H. Lieu, S. Oeser, H. Bennett, P. Rigault, D. Barker, T. K. McDaniel and M. S. Chee, *Genome Res.*, 2004, **14**, 2347–2356.
4 N. V. Zaytseva, V. N. Goral, R. A. Montagna and A. J. Baeumner, *Lab Chip*, 2005, **5**, 805–811.
5 H. Andersson, W. van der Wijngaart, P. Enoksson and G. Stemme, *Sens. Actuators, B*, 2000, **67**, 203–208.
6 K. Sato, M. Tokeshi, T. Odake, H. Kimura, T. Ooi, M. Nakao and T. Kitamori, *Anal. Chem.*, 2000, **72**, 1144–1147.
7 M. Zimmermann, S. Bentley, H. Schmid, P. Hunziker and E. Delamarche, *Lab Chip*, 2005, **5**, 1355–1359.
8 G. M. Walker and D. J. Beebe, *Lab Chip*, 2002, **2**, 131–134.
9 E. Berthier, J. Warrick, H. Yu and D. J. Beebe, *Lab Chip*, 2008, **8**, 852–859.
10 E. Berthier, J. Warrick, H. Yu and D. J. Beebe, *Lab Chip*, 2008, **8**, 860–864.
11 D. R. Gossett, W. M. Weaver, A. J. Mach, S. C. Hur, H. T. K. Tse, W. Lee, H. Amini and D. Di Carlo, *Anal. Bioanal. Chem.*, 2010, **397**, 3249–3267.
12 H. M. Ji, V. Samper, Y. Chen, C. K. Heng, T. M. Lim and L. Yobas, *Biomed. Microdevices*, 2007, **10**, 251–257.
13 M. C. Park, J. Y. Hur, K. W. Kwon, S. H. Park and K. Y. Suh, *Lab Chip*, 2006, **6**, 988–994.
14 E. Berthier and D. J. Beebe, *Lab Chip*, 2007, **7**, 1475–1478.
15 J. Ju, J. Y. Park, K. C. Kim, H. Kim, E. Berthier, D. J. Beebe and S. H. Lee, *J. Micromech. Microeng.*, 2008, **18**, 087002.
16 R. Bhardwaj, X. H. Fang, P. Somasundaran and D. Attinger, *Langmuir*, 2010, **26**, 7833–7842.